ISSN 2635-1676, Nanobiotechnology Reports, 2024, Vol. 19, No. 2, pp. 269–274. © Pleiades Publishing, Ltd., 2024.
Russian Text © The Author(s), 2024, published in Rossiiskie Nanotekhnologii, 2024, Vol. 19, No. 3, pp. 390–395.

DEVICES AND PRODUCTS BASED ON NANOMATERIALS AND NANOTECHNOLOGIES

Operando Cell for Synchrotron Studies of Gas Sensors

M. A. Gritsai[a,*], V. A. Polyakov[a], P. V. Medvedev[a], Yu. Yu. Zhityaeva[b], O. I. Il'in[b], and M. A. Soldatov[a]

[a] *Smart Materials Research Institute, Southern Federal University, Rostov-on-Don, Russia*

[b] *Institute of Nanotechnologies, Electronics, and Instrumentation Technology, Southern Federal University, Taganrog, Russia*

**e-mail: gritsai@sfedu.ru*

Received December 19, 2023; revised December 19, 2023; accepted December 26, 2023

Abstract—A cell for conducting operando measurements of X-ray absorption spectra for gas-sensitive sensors based on ZIF-8/ZIF-67 nanofilms is developed and fabricated. The cell is made of stainless steel, which makes it possible to study, among other things, corrosive gases. The possibility of heating and continuous measurement of the sensor temperature during an operando experiment to evaluate the dynamics of sorption in the processes of heating/cooling the cell. The isolated sensor holder has contacts for measuring the capacitance/resistance of the sensor. To measure X-ray absorption spectra for gas-sensitive gas-sensor materials, an X-ray transparent window is provided. For sensors based on ZIF-8 and ZIF-67 nanofilms, the X-ray absorption spectra are measured for the *K* edges of Zn and Co, respectively. It is found that after exposure to NO_2 in a gas-sensitive material based on ZIF-8/ZIF-67 nanofilms, long-range order is lost and the film undergoes amorphization. The X-ray absorption spectra measured for a gas-sensitive material based on ZIF-8/ZIF-67 nanofilms before and after exposure to NO_2 indicate a change in the local atomic and electronic structures near cobalt atoms.

DOI: 10.1134/S2635167624600810

INTRODUCTION

Gas sensors are key components of household items that improve quality of life [1, 2]. They are designed to detect and quantify the presence of various gases in the environment, the household, and during technological processes [3–5]. Their importance in the modern world cannot be overestimated, since they perform a signaling function, providing information about unwanted or dangerous leaks of toxic and explosive gases. Thus, semiconductor gas sensors are capable of detecting flammable gases in the air, such as hydrogen [6], methane [7], and other liquefied hydrocarbon gases [7]. Air humidity sensors are indispensable in the food industry [8], and oxygen detection is important, for example, for monitoring automobile exhaust emissions [9], as well as in various metallurgical processes [10]. One of the most serious environmental problems caused by the growing technogenic influence of humans on nature is the release of toxic gases into the atmosphere: oxides of nitrogen, sulfur and carbon, which actively destroy the ozone layer [11]. Interacting with atmospheric moisture, nitrogen and sulfur oxides form acid rain, causing the corrosion of metal structures and changes in the acidity of soil and water bodies [12, 13]. All these factors harm agriculture and fisheries [14, 15]. Thus, the development of sensors for the determination of NO_x, SO_x, and CO is a pressing issue [16, 17].

A gas sensor must have two main functions: a receptor function (recognition of a specific gas) and a transducer function (conversion of the signal from the gas-receptor interaction into a sensory signal, for example, electrical signal) [18–20]. The most widespread are solid-state gas sensors in which the gas–receptor interaction is reduced to physisorption/chemisorption or electrochemical reaction [21]. Thus, it is convenient to convert the interaction of a gas with semiconductor oxides into a change in the electrical resistance of the converter, and the interaction of a gas with dielectrics into a change in the capacitance of the converter [22].

Nanomaterials such as nanowires [23], nanoparticles [24, 25], nanotubes [26], and nanofilms [27] can also be used in the development of sensors. Their functionalization can significantly increase sensitivity and selectivity [28–30]. The advantage of nanofilms is their uniform application on the sensor surface. One of the promising classes of new materials for creating sensors are metal-organic frameworks (**MOF**) [31–34]. These materials consist of metal ions or metal clusters interconnected into a three-dimensional porous framework using bridging organic molecules,

i.e., linkers [35]. In this case, the pore size and specific surface area can be varied by changing the type of linker. Thanks to this modular structure, it becomes possible to finely regulate the selectivity of the material to certain molecules, and a high porosity increases the efficiency of interaction of the material with a gas [36]. ZIF-8 is an organometallic analogue of natural framework aluminosilicates, i.e., zeolites [37]. However, unlike their natural counterparts, the ZIF-8 family of MOFs are constructed from zinc ions coordinated by the nitrogen atoms of 2-methylimidazole. The result is a frame with a high specific surface area of up to 2000 m^2/g, and relative thermal and chemical stability [38]. The isomorphic substitution of zinc with divalent cobalt leads to the formation of a similar structure due to the proximity of the ionic radii of Zn(II) and Co(II) [39].

Understanding how gases interact with ZIF is of paramount importance to optimize sensor performance under various operating conditions, increasing its sensitivity, selectivity, and durability [40, 41]. X-ray absorption spectroscopy (**XAS**) is an effective method for studying the local atomic and electronic structure with elemental selectivity. Using XAS, it is possible to study nanofilms under the influence of gas flows and evaluate changes in the local environment and the oxidation state of metal atoms that make up the MOF [42]. However, conducting research under technological conditions (operando) requires specialized measuring cells and access to synchrotron-radiation sources. In particular, the tightness of the measuring cell and the possibility of supplying a gas mixture. Sorption processes greatly depend on temperature [43], so it is necessary to ensure the possibility of heating and continuous measurement of the sensor temperature during operando experiment to evaluate the dynamics of sorption in the processes of heating/cooling the cell. In addition, the cell must have contacts for measuring the capacitance/resistance of the sensor. To measure the X-ray absorption spectra for gas-sensitive gas-sensor materials, it is necessary to provide a window transparent to X-rays.

The purpose of this work is to create a cell for measuring the X-ray absorption spectra in operando. Gas sensors based on ZIF-8/ZIF-67 nanofilms are chosen as the test samples.

MANUFACTURING A GAS-SENSITIVE SENSOR

Contact tracks on glass were fabricated according to a previously described protocol [44, 45]. Using magnetron sputtering, a three-layer structure was formed based on Cr (15 nm)/Cu (100 nm)/Cr (15 nm) metal films. The topology of the electrodes was created by photolithography using an MJB4 exposure setup (SUSS, Switzerland). The photomask design was developed based on an interdigitated array (IDA) electrode structure. The width of the electrodes was equal to the gap between them and amounted to 200 μm. The size of the gaskets for connecting the measuring equipment was 2.5 mm^2. The multilayer film structure was etched with HCl-based solutions: $HCl : H_2O$ (1 : 1) for Cr and $H_3PO_4 : HNO_3 : CH_3COOH : H_2O$ (45 : 2 : 9 : 3) for Cu.

A layer of gas-sensitive material based on ZIF-8/ZIF-67 was applied to the contact tracks in accordance with the procedure described in [46]. To clean the surface of the chip, it was immersed in hexane and sonicated for 10 min. The chip was then air dried, washed with acetone, and dried again. After this, the chip was immersed for 30 min in a solution prepared by mixing 10 mL of a 25-mmol solution of zinc nitrate (for ZIF-8) or divalent cobalt (for ZIF-67) in methanol and 10 mL of a 50-mmol solution of 2-methylimidazole in methanol. Next, the chip was removed from the solution and washed with pure methanol.

DEVELOPMENT OF OPERANDO CELLS

A CAD model of the gas cell was designed using a computer-aided design system and is available for download. The cell body and covers (Fig. 1a) are made of AISI-304 steel. The cell body is a single piece with dimensions of 60 × 60 mm and a thickness of 15 mm. In the center of the piece there is a hole in the form of a superellipse; a chip with a gas-sensitive coating is placed in this area on a holder made of F4 fluoroplastic. Tubes for supplying and discharging gases are also connected to this area. Another hole in the top of the main piece is made to connect the contacts to a gas sensor to measure changes in the resistance between the contacts of the chip. The reaction zone was hermetically sealed on both sides with tight lids with windows made of a material transparent to X-ray radiation (Kapton). Two heating elements are inserted into the body of the cell.

Figure 1b shows a diagram for measuring the X-ray absorption spectra during gas injection into a gas cell. The experimental gas cell was tested at the structural-materials research station of the Kurchatov synchrotron radiation source (electron-beam energy of 2.5 GeV, storage-ring current in the range of 50–120 mA). A double-crystal Si (220) monochromator was used to extract the energy of incident photons. The measurements were carried out in the fluorescence-output-detection mode.

Before measurements, the cell was filled with CO and heated to 180°C. Figure 2 shows the X-ray absorption spectrum for the *K*-edge of cobalt measured using the developed gas cell for a gas-sensitive material based on ZIF-8/ZIF-67 nanofilms.

To record changes in the local atomic and electronic structure of the sensor material, we studied the sample's reaction to NO_2 of various concentrations (Fig. 3a) at a temperature of 180°C. Using an Agilent E4980A impedance meter, changes in the electrical

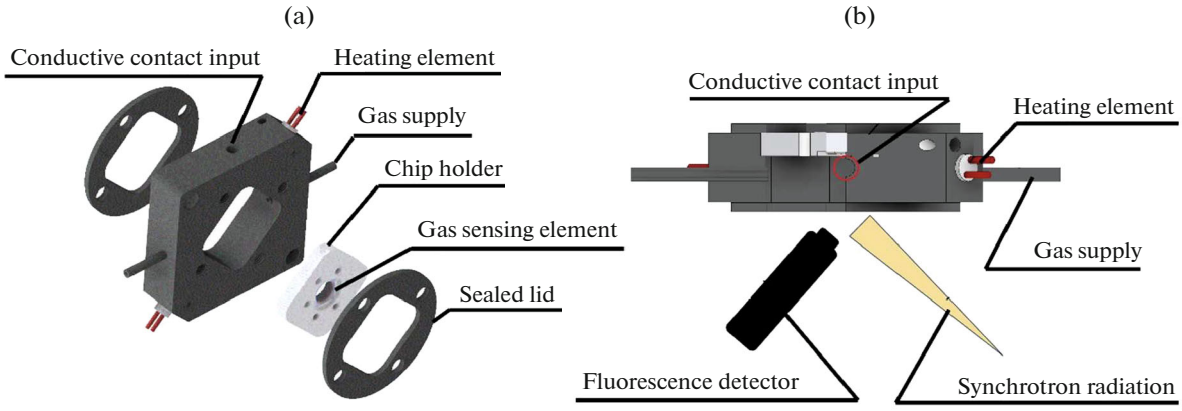

Fig. 1. Diagram of a gas cell for measuring the X-ray absorption spectra for gas-sensitive materials in operando (a); experimental scheme (b).

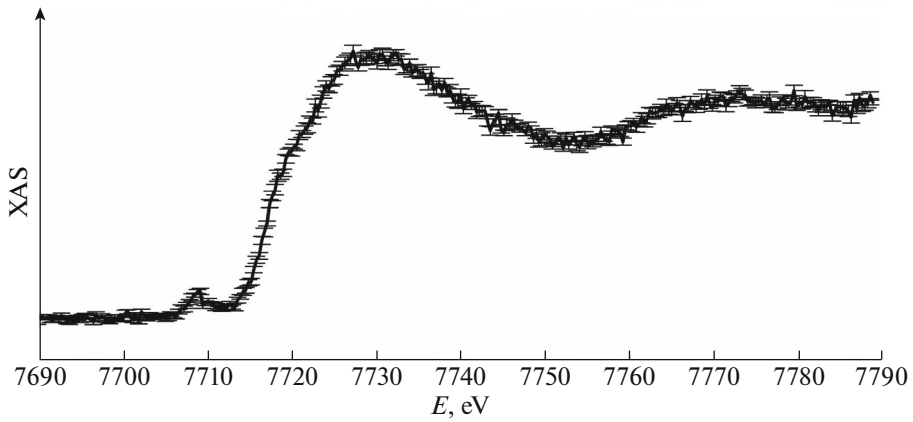

Fig. 2. Total spectrum for *K* absorption edge of cobalt recorded in the developed gas cell.

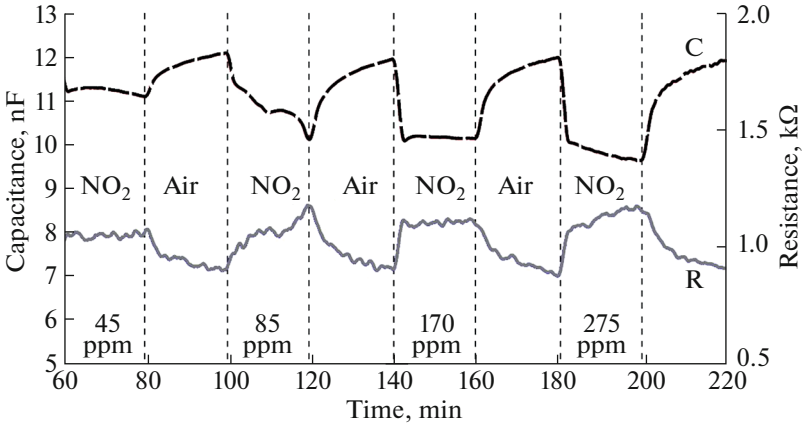

Fig. 3. Sensor response to the supply of NO_2 of various concentrations.

characteristics of the gas-sensitive film were studied. The measurement was carried out at a frequency of 100 Hz and a voltage of 1 V. As a result of processing the data obtained (Fig. 3), the values of the capacitive and resistive sensitivity of the sample to various concentrations of NO_2 are summarized in Table 1.

Table 1. Resistive (S_R) and capacitive (S_C) sensor sensitivity to NO_2 of different concentrations

NO_2 concentration, ppm	Sensitivity, %	
	S_R	S_C
25		0.001
45	3.87674	6.52156
85	14.28571	14.65482
170	15.30398	17.60784
275	19.17373	20.00164

From Table 1 it can be seen that with increasing concentration of NO_2 from 45 to 275 ppm the signal S_R and S_C increases from 3 to 19 and from 6 to 20%, respectively. At the same time, the strong nonlinearity in the change in the capacitance and resistance, when NO_2 is supplied at a concentration of 25 ppm, did not allow us to evaluate the sensor response at the given gas concentration. Also, when a gas concentration of 85 ppm was supplied, transient processes were observed when the capacitive and resistive signals changed, which may be due to changes in the structure of the film itself.

STABILITY OF THE STRUCTURE OF THE GAS-SENSITIVE MATERIAL AFTER NO_2 TREATMENT

The color of the sensor material after interaction with NO_2 changed to brown. Analysis of the diffraction patterns before and after NO_2 treatment showed disruption of the crystallinity of the ZIF-8/ZIF-67 nanofilms. Before sample processing, the diffraction pattern clearly shows peaks corresponding to the ZIF-8/ZIF-67 structures (7°, 10°, 13°, 15°), however after treatment with NO_2 the diffraction pattern exhibited only a broad peak of amorphous silica and peaks corresponding to metallic copper from the contact tracks (Fig. 4a). Whereas the chip continues to work as a sensor after repeated NO_2 processing, it can be assumed that the ZIF-8/ZIF-67 phase has become amorphous, losing long-range order.

Sample S2 is a chip coated with three layers of ZIF-8 and three layers of ZIF-67. Figure 4b shows the X-ray absorption spectra measured for crystalline ZIF-67, ZIF-67 deposited onto the contact tracks in the form of a nanofilm, and ZIF-67 deposited onto the contact tracks in the form of a nanofilm after exposure to NO_2. It can be seen that the intensity of the pre-edge feature at an energy of ~7705 eV and the shape of the main maximum at an energy of 7730 eV for crystalline ZIF-67 and ZIF-67 deposited onto the contact tracks in the form of a nanofilm practically coincide, which may indicate identical local atomic and electronic structures. However, after exposure to NO_2 the pre-edge feature disappears and the intensity of the main maximum increases, which indicates a change in the local environment of cobalt atoms.

It is known that even at room temperature NO_2 can exhibit oxidative functions and therefore become an electron acceptor. When NO_2 comes into contact with ZIF-8 and ZIF-67 films, electrons are lost, as a result, the number of holes in the MOF film increases, which, together with the high activity of NO_2 leads to a decrease in the resistance [41]. On the other hand, it is known that the cobalt(II) ion has a $3d^7$ electronic level containing a free orbital. As a result, it becomes possible for electrons to migrate inside the *d* sublevel. In a zinc ion, the outer electron layer has the electron configuration $3d^{10}$, which means there is no vacant *d*

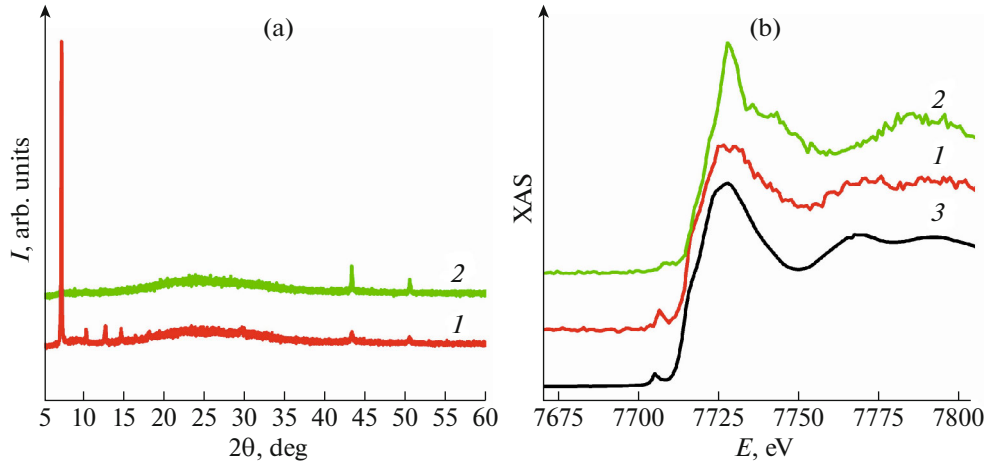

Fig. 4. X-ray diffraction profiles of samples S_2 before (*1*) and after (*2*) NO_2 processing (a). X-ray absorption spectra obtained for chips after exposure to NO_2 compared to the original coating for Co: (*1*) S_2 before NO_2 treatment, (*2*) S_2 after NO_2 treatment, (*3*) crystalline ZIF-67 (b).

orbitals. As a result, when moving from zinc to cobalt, the electrical conductivity increases.

The functionalization of ZIF-8 with layers of ZIF-67 results in increased sensitivity and magnitude of the sensor response. This may be due to a decrease in the activation energy due to an increase in temperature to 180°C, resulting in an increase in the efficiency of electron transfer of NO_2 donor impurities, which ensures a high conductivity of the sensitive layer. At the same time, ZIF-67 layers contribute to an increase in impedance due to the formation of additional capacitances, which affects the overall resistance of the structure and its response when gases are supplied. Moreover, a gas with the same concentration causes different levels of capacitive and resistive response of the sensor.

CONCLUSIONS

A cell has been developed for measuring the X-ray absorption spectra for gas-sensitive materials in operando. The cell allows heating of the gas sensor, the creation of an atmosphere of various gases, and measurement of the resistance and capacitance of the gas sensor. The X-ray absorption spectra were recorded for the *K* edge of cobalt and zinc using the developed gas cell for a gas-sensitive material based on ZIF-8/ZIF-67 nanofilms. Based on the analysis of X-ray diffraction data, it was established that after exposure to NO_2 in the MOF structure, long-range order is lost and amorphization of the film occurs, while the sensor retains its functionality and its sensitivity to NO_2. The X-ray absorption spectra measured for a gas-sensitive material based on ZIF-8/ZIF-67 nanofilms before and after exposure to NO_2, indicate a change in the local atomic and electronic structures near the cobalt atoms.

FUNDING

The study was supported by the Russian Science Foundation (grant no. 22-29-01124) at the Southern Federal University.

CONFLICT OF INTEREST

The authors of this work declare that they have no conflicts of interest.

REFERENCES

1. C. Wang, L. Yin, L. Zhang, et al., Sensors (Basel) **10**, 2088 (2010). https://doi.org/10.3390/s100302088
2. G. Eranna, B. C. Joshi, D. P. Runthala, and R. P. Gupta, Crit. Rev. Solid State Mater. Sci. **29**, 111 (2004).
3. E. Llobet, Sens. Actuators, B **179**, 32 (2013). https://doi.org/10.1016/j.snb.2012.11.014
4. G. Eranna, B. C. Joshi, D. P. Runthala, and R. P. Gupta, Crit. Rev. Solid State Mater. Sci. **29,** 111 (2004). https://doi.org/10.1080/10408430490888977
5. A. Dey, Mater. Sci. Eng. B **229**, 206 (2018). https://doi.org/10.1016/j.mseb.2017.12.036
6. H. Gu, Z. Wang, and Y. Hu, Sensors **12**, 5517 (2012). https://doi.org/10.3390/s120505517
7. G. Jiménez-Cadena, J. Riu, and F. X. Rius, Analyst **132**, 1083 (2007). https://doi.org/10.1039/B704562J
8. H. Farahani, R. Wagiran, and M. N. Hamidon, Sensors **14**, 7881 (2014). https://doi.org/10.3390/s140507881
9. M. Al-Hashem, S. Akbar, and P. Morris, Sens. Actuators, B **301**, 126845 (2019). https://doi.org/10.1016/j.snb.2019.126845
10. H. Yuan, S. A. A. A. Aljneibi, J. Yuan, et al., Adv. Mater. **31**, 1807161 (2019). https://doi.org/10.1002/adma.201807161
11. I. Manisalidis, E. Stavropoulou, A. Stavropoulos, and E. Bezirtzoglou, Front. Public Health **8**, 14 (2020). https://doi.org/10.3389/fpubh.2020.00014
12. T. Boningari and P. G. Smirniotis, Curr. Opin. Chem. Eng. **13**, 133 (2016). https://doi.org/10.1016/j.coche.2016.09.004
13. K. Wetchakun, T. Samerjai, N. Tamaekong, et al., Sens. Actuators, B **160**, 580 (2011). https://doi.org/10.1016/j.snb.2011.08.032
14. K. W. T. Goulding, Soil Use Manage. **32**, 390 (2016). https://doi.org/10.1111/sum.12270
15. V. Eyring, I. S. A. Isaksen, T. Berntsen, et al., Atmos. Environ. **44**, 4735 (2010). https://doi.org/10.1016/j.atmosenv.2009.04.059
16. X. Zhou, S. Lee, Z. Xu, and J. Yoon, Chem. Rev. **115,** 7944 (2015). https://doi.org/10.1021/cr500567r
17. H.-Y. Li, S.-N. Zhao, S.-Q. Zang, and J. Li, Chem. Soc. Rev. **49,** 6364 (2020). https://doi.org/10.1039/C9CS00778D
18. H. Nazemi, A. Joseph, J. Park, and A. Emadi, Sensors **19**, 1285 (2019). https://doi.org/10.3390/s19061285
19. T. Wang, Y. Guo, P. Wan, et al., Small **12**, 3748 (2016). https://doi.org/10.1002/smll.201601049
20. J. Zhang, Z. Qin, D. Zeng, and C. Xie, Phys. Chem. Chem. Phys. **19,** 6313 (2017). https://doi.org/10.1039/C6CP07799D
21. A. Šutka and K. A. Gross, Sens. Actuators, B **222**, 95 (2016). https://doi.org/10.1016/j.snb.2015.08.027
22. J. van den Broek, S. Abegg, S. E. Pratsinis, and A. T. Güntner, Nat. Commun. **10**, 4220 (2019). https://doi.org/10.1038/s41467-019-12223-4
23. X. Chen, C. K. Y. Wong, C. A. Yuan, and G. Zhang, Sens. Actuators, B **177**, 178 (2013). https://doi.org/10.1016/j.snb.2012.10.134
24. S. Agarwal, P. Rai, E. N. Gatell, et al., Sens. Actuators, B **292**, 24 (2019). https://doi.org/10.1016/j.snb.2019.04.083

25. M. S. Chavali and M. P. Nikolova, SN Appl. Sci. **1**, 607 (2019). https://doi.org/10.1007/s42452-019-0592-3
26. M. N. Norizan, M. H. Moklis, DemonS. Z. Ngah, et al., RSC Adv. **10**, 43704 (2020). https://doi.org/10.1039/D0RA09438B
27. J. Wang, H. Shen, Y. Xia, and S. Komarneni, Ceram. Int. **47**, 7353 (2021). https://doi.org/10.1016/j.ceramint.2020.11.187
28. T. Kida, A. Nishiyama, Z. Hua, et al., Langmuir **30**, 2571 (2014). https://doi.org/10.1021/la4049105
29. M. Masikini, M. Chowdhury, and O. Nemraoui, J. Electrochem. Soc. **167**, 037537 (2020). https://doi.org/10.1149/1945-7111/ab64bc
30. W. Zheng, C. Yang, Z. Li, et al., Sens. Actuators, B **329**, 129127 (2021). https://doi.org/10.1016/j.snb.2020.129127
31. H. Yuan, N. Li, W. Fan, et al., Adv. Sci. **9**, 2104374 (2022). https://doi.org/10.1002/advs.202104374
32. L. Wang, Sens. Actuators, A **307**, 111984 (2020). https://doi.org/10.1016/j.sna.2020.111984
33. M.-S. Yao, W.-H. Li, and G. Xu, Coord. Chem. Rev. **426**, 213479 (2021). https://doi.org/10.1016/j.ccr.2020.213479
34. W.-T. Koo, J.-S. Jang, and I.-D. Kim, Chemistry **5**, 1938 (2019). https://doi.org/10.1016/j.chempr.2019.04.013
35. H. Furukawa, K. E. Cordova, M. O'Keeffe, and O. M. Yaghi, Science **341,** 1230444 (2013). https://doi.org/10.1126/science.1230444
36. J. L. C. Rowsell and O. M. Yaghi, J. Am. Chem. Soc. **128**, 1304 (2006). https://doi.org/10.1021/ja056639q
37. S. Tanaka, K. Fujita, Y. Miyake, et al., J. Phys. Chem. C **119**, 28430 (2015). https://doi.org/10.1021/acs.jpcc.5b09520
38. K. Zhou, B. Mousavi, Z. Luo, et al., J. Mater. Chem. A **5**, 952 (2017). https://doi.org/10.1039/C6TA07860E
39. W. Sun, X. Zhai, and L. Zhao, Chem. Eng. J. **289**, 59 (2016). https://doi.org/10.1016/j.cej.2015.12.076
40. E.-X. Chen, H. Yang, and J. Zhang, Inorg. Chem. **53**, 5411 (2014). https://doi.org/10.1021/ic500474j
41. E.-X. Chen, H.-R. Fu, R. Lin, et al., ACS Appl. Mater. Interfaces **6**, 22871 (2014). https://doi.org/10.1021/am5071317
42. F. de Groot, Chem. Rev. **101**, 1779 (2001). https://doi.org/10.1021/cr9900681
43. F. E. Bartell, T. L. Thomas, and Y. Fu, J. Phys. Chem. **55**, 1456 (1951). https://doi.org/10.1021/j150492a005
44. I. Safi, Surf. Coat. Technol. **127**, 203 (2000). https://doi.org/10.1016/S0257-8972(00)00566-1
45. J. Musil, P. Baroch, J. Vlcek, et al., Thin Solid Films **475**, 208 (2005). https://doi.org/10.1016/j.tsf.2004.07.041
46. A. M. Aboraia, A. A. A. Darwish, V. Polyakov, et al., Opt. Mater. **100**, 109648 (2020). https://doi.org/10.1016/j.optmat.2019.109648